Non-Contact Probes for On-Wafer Characterization of Sub-millimeter Wave Devices and Integrated Circuits

Cosan Caglayan, *Student Member, IEEE,* Georgios C. Trichopoulos, *Member, IEEE,* and Kubilay Sertel, *Senior Member, IEEE*

Abstract—We present a novel, non-contact metrology approach for on-wafer characterization of sub-millimeter wave devices, components, and integrated circuits. Unlike existing contact probes that rely on small metallic tips that make physical contact with the device on the chip, the new non-contact probes are based on electromagnetic coupling of vector network analyzer (VNA) test ports into the coplanar waveguide environment of integrated devices and circuits. Efficient signal coupling is achieved via a quasi-optical link between the VNA ports and planar antennas that are monolithically integrated with the test device. Experimental validation of the non-contact device metrology system is presented for the first time to demonstrate the accuracy and repeatability of proposed approach for the 325-500 GHz (WR 2.2) and 500-750 GHz (WR 1.5) bands.

I. INTRODUCTION

RECENT advances in compound semiconductor materials and processing techniques are enabling extremely fast electronic devices that could realize ultra-fast electronics and "bridge" the so-called THz gap, joining the microwave and infrared ends of the electromagnetic spectrum. Among the key applications that drive ultra-high-speed electronics are deep space spectroscopy [1], medical, pharmaceutical and security imaging [2], [3] and high-speed communications [4]. However, current state-of-the-art terahertz systems are large, expensive and bulky, such as backward wave oscillators (BWOs) and femtosecond laser-based photomixers. The steep cost of such systems is one of the key factors slowing the proliferation of THz sensing and spectroscopy applications. All-electronic integrated systems that can provide ultrafast switching (>1 THz) are desperately needed to develop compact and cost effective solutions.

Among recent developments in high-speed device topologies are high electron mobility transistors (HEMTs) on III-V low band gap semiconductors, such as InP. These ultrafast transistors have already achieved 650 GHz operation [5] for mixers, amplifiers, and low-noise oscillators. Aggressive scaling of the transistor gate lengths to reduce electron transit time and novel ohmic contact techniques that reduce detrimental parasitics resulted in significant device gain at frequencies

approaching the 1 THz barrier. Nonetheless, a design trade-off between power handling and fast switching is typically encountered with conventional device topologies. To address this bottleneck and further extend device performance to the THz band, novel and unconventional device topologies, such as plasma wave field effect transistors (FETs) [6] and heterostructure resonant tunneling devices are being investigated. However, reliable fabrication of such new device topologies remains an active research area.

Perhaps more importantly, testing and characterization of these new devices has been a challenge at their intended operation frequencies. Characterization of THz monolithic integrated circuits (TMICs) is either performed in a waveguide environment after packaging [7], or directly on the device chip using expensive, high-frequency contact probes. Obviously, on-wafer characterization of these state-of-the-art devices is crucial since measurements after packaging do not reflect the native performance of the device or the integrated circuit. The latter is primarily due to inefficient coupling and poor bandwidth between coplanar environment of the device and the conventional waveguide blocks [7].

As noted above, contact probes are used for on-chip device characterization. For frequencies beyond 100 GHz, waveguide-based frequency extenders are used in conjunction with conventional vector network analyzers (VNAs). Due to the waveguide topology, the measurement bandwidths of these probes
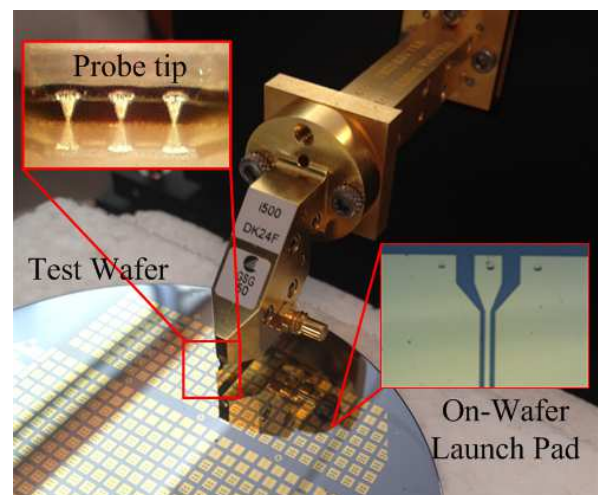

Fig. 1. A contact probe landed on chip under test, the launch pad and scuff marks on the chip are shown in the inset.

are limited to the fundamental waveguide mode frequencies. The ground-signal-ground (GSG) probe tip is carefully transitioned to the waveguide flange to minimize insertion losses. A typical on-wafer measurement setup using contact probes is shown in Fig. 1. As seen, the probe requires a physical contact with the chip under test. They are typically fabricated in form of thin silicon chips (Dominion MicroProbes Inc.), thin-film microstip lines (Cascade Microtech Inc.) or micro-coaxial transmission lines (GGB Industries) that require micromachining or microfabrication. Also, the probe tips are affixed to the probe body via mechanical clamping. As such, they are susceptible to vibrations in the measurement setup and flex under stress during contact. In addition, the sharp tips are often used to break through the thin passivation layers on the wafer to make electrical contact with the pads. This process puts undue physical stress on the probe tips, further limiting the lifetime of contact probes. More importantly for THz-frequency probes, unless the contact force between the probe tip and test chip is kept under a threshold value, tip metallizations typically wear off, resulting in detrimental mismatches. At this point the damaged probe tips need to be replaced by the vendor to restore performance.

Under ideal conditions, contact probes can be very effective and exhibit long life cycles. For instance, DMPI Inc. rates their probes to 10,000s of contact cycles. However, we note that this rating is for a controlled setup where the contact force is precisely kept below a certain threshold [8]. In practice, human operator can easily exceed the threshold for the contact force and damage the probe tip. Research efforts continue to circumvent this drawback of conventional contact probes. For instance in [9], an integrated strain sensor is used as a feedback device to control and monitor the contact force and planarity angle in order to mitigate the fragility issues mentioned above.

Conventional contact probes are also rather expensive and commercially only available up to 1 THz. Further scaling of probe tips exacerbates fragility and cost issues. In an effort to circumvent these shortcomings of contact probes, we recently proposed a novel technique that enables non-contact characterization of on-chip components. In [10] and [11], we presented the first results pertaining to one-port non-contact measurements. In this paper, we demonstrate both one-port and two-port calibration and measurement capability with non-contact probes for the first time along with a preliminary repeatability study.

As outlined in detail in the next section, the non-contact probes can achieve an efficient quasi-optical coupling between VNA test ports and coplanar environment of the device under test without having any physical contact. This contact-free link is achieved via radiative coupling of test ports onto the planar slot antennas that are monolithically integrated with the device. To enable accurate S-parameters measurements, repeatable errors due to reflections and losses in the non-contact test-bed must be calibrated using on-wafer standards. For this purpose, shorted coplanar waveguide (CPW) lines with varying electrical lengths are used, as described in [12].

In the following, we present the non-contact probe setup in detail and demonstrate its performance for on-chip S parameter measurements. The paper is organized as follows: Section
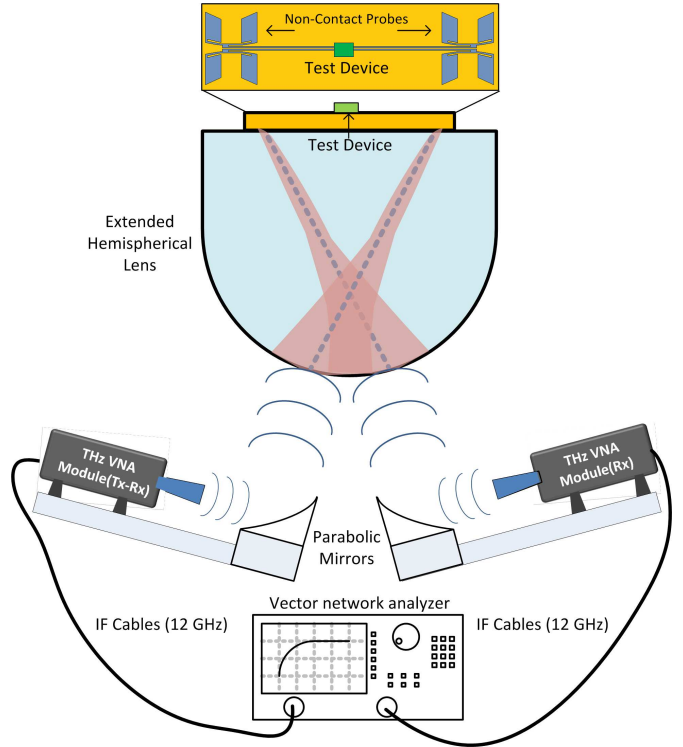

Fig. 2. Illustration of the non-contact probe setup [11]

2 describes the concept and operation principles of the non-contact probe and its implementation. In Section 3, we develop a simple and accurate calibration approach using the offset short method [12]. In Section 4, the insertion loss performance of the non-contact probes is compared with the commercially available contact probes. Section 5 demonstrates the accuracy of the new non-contact probes system via impedance characterization of an on-chip antenna for 325-500 GHz and 500-750 GHz bands. In addition, we present, for the first time, two-port S-parameter characterization of two passive components in the 325-500 GHz band using our non-contact approach.

II. THz Non-Contact Probe Setup: Concept and Implementation

Conventionally, on-wafer S-parameter measurements in the mmW band are performed using a vector network analyzer (VNA) and coaxial cables connecting the VNA ports to contact probes. Since current coaxial cable technology is limited to 110 GHz, for higher frequencies, waveguide-coupled VNA ports must be used. To do so, high frequency transceiver modules are utilized to extend the VNA frequency range up to and beyond 1 THz. The waveguide ports of the frequency extenders can either be interfaced with high-frequency contact probes for on-wafer measurements (transition from waveguide to CPW) or they can be coupled to free space via conical or diagonal horn antennas for transmission/reflection measurements.

The novel technique presented here for on-chip device testing eliminates the need for physical contact with test wafer and avoids the various drawbacks and shortcomings of contact probes. Operation principle of the "non-contact" probes can
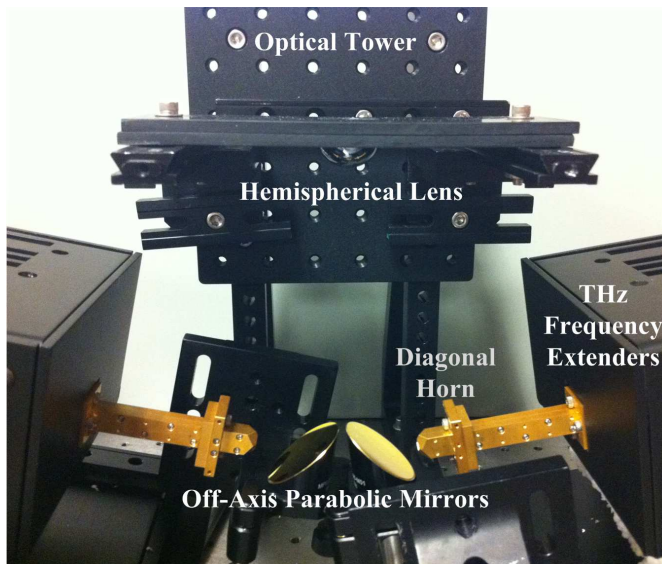
Fig. 3. Prototype of the non-contact probes setup

be conceptually described based on the illustration in Fig. 2 where the test device as shown in the figure inset:

The incident beam is launched from the horn antenna attached to a THz VNA extender module and coupled onto a planar antenna using a hemispherical lens focused on the antenna. The signal reflected from the device is transmitted back by the incident antenna which then re-radiates back to the horn antenna of port 1. This enables reflection measurements (S_{11} and S_{22}) of the device. The signal transmitted from the test device is coupled-out by a second antenna connected to the output port of the device which radiates back to the second VNA port, enabling transmission measurements (S_{12}, S_{21}).

To achieve efficient coupling onto and out of the test wafer, the radiation pattern of planar on-wafer antennas as well as the quasi-optical link alignment must be optimized. We should remark that in Fig. 2 the incident and transmitted beam angles are exaggerated to underline the physical principle of the non-contact probes concept. In reality, the incident and transmitted beam angles are quite small (<10 degrees), thus allowing effective coupling to planar antennas at broadside.

Our approach takes advantage of the high Gaussicity (>85%) [13] of both the horn antennas at the output of VNA frequency extenders and the double-slot antennas on the test wafer (with Gaussicity >60%) [14]. The resulting quasi-optical system can efficiently couple waveguide ports of the extension modules into the CPW environment of integrated devices or circuits. With this new approach, the need for physical contact is completely eliminated.

Concisely, the proposed non-contact THz probe comprises of two key features: i) a quasi-optical setup for the effective radiative coupling between on-chip planar antennas and the test ports of a standard vector network analyzer (VNA), ii) broadband, butterfly shaped double-slot antennas integrated with the device on the test wafer. The abovementioned quasi-optical setup can be implemented in many different configurations. The prototype shown in Fig. 3 is one such implementation using commercially available optomechanical

components. Here, the incident beam direction is controlled by placing THz VNA modules on inclined surfaces. The beam is reflected perpendicularly using 90° off-axis parabolic mirrors resulting in a collimated Gaussian beam as desired. The extended hemispherical lens [14] is placed in a custom lens holder affixed to an optical tower with adjustable height. The height of the lens does not affect the coupling efficiency significantly since the beam is collimated by the parabolic mirror.

Accurate alignment of the quasi-optical sub-system in the non-contact probe setup is of utmost importance to minimize insertion loss and maximize the overall probe dynamic range. This procedure can be challenging since unlike visible light, the mmW and THz frequencies are not directly observable with naked eye. In our setup, we follow an iterative procedure using the time-domain response of the return signal to align the input port of the non-contact probe setup.

To so do, first the frequency extenders are calibrated to the waveguide output flange using the vendor-supplied offset short calibration set (1st tier calibration). Next, one of the offset-short standards are placed at the focal plane of the hemispherical lens, approximately at the position of the expected beam focus. After this first tier calibration, the S_{11} response is monitored in time domain on the VNA screen. At this step, the reflection from the curved lens surface is clearly visible as a distinct peak in the time-domain signal. By shifting the frequency extender position, the initial reflection peak from the curved lens surface adjusted to align with the desired distance. Following this step, the position of the calibration substrate at the focal plane of the hemispherical lens is adjusted to maximize the reflection from the CPW offset short termination. Subsequent adjustments to the alignment are aimed at successively improving the reflected signal magnitude (in time domain) by adjusting the positioning of the off-axis parabolic mirrors as well as the relative positions of the hemispherical lens and the calibration substrate. After the desired alignment is achieved, the location of the non-contact probe antenna on the calibration substrate is the same as the position of the beam focus on the lens focal plane. This iterative method is akin to typical optical alignment process of lens trains that are routinely used in optical and infrared laser-based systems.

Once the input port is aligned to desired performance, a similar procedure is applied for the second port for two-port measurements. Often, further adjustments to the first port alignment is required to optimize the performance for two-port measurements. It is important to note that once the quasi-optical system is aligned, all measurements (including the calibration data) are collected using the same quasi-optical sub-system. As such, the quasi-optical sub-system does not induce any non-repeatable uncertainty in the measured data. We also note that the frequency extenders are only available for sub-bands (e.g., 90-140 GHz, 140-220 GHz, 220-325 GHz, 325-500 GHz, 500-750 GHz, and 750-1150 GHz). Nonetheless, as long as the horn antennas of the extender modules are kept at the same location in the quasi-optical setup, no additional changes are required for the non-contact probes between frequency bands.

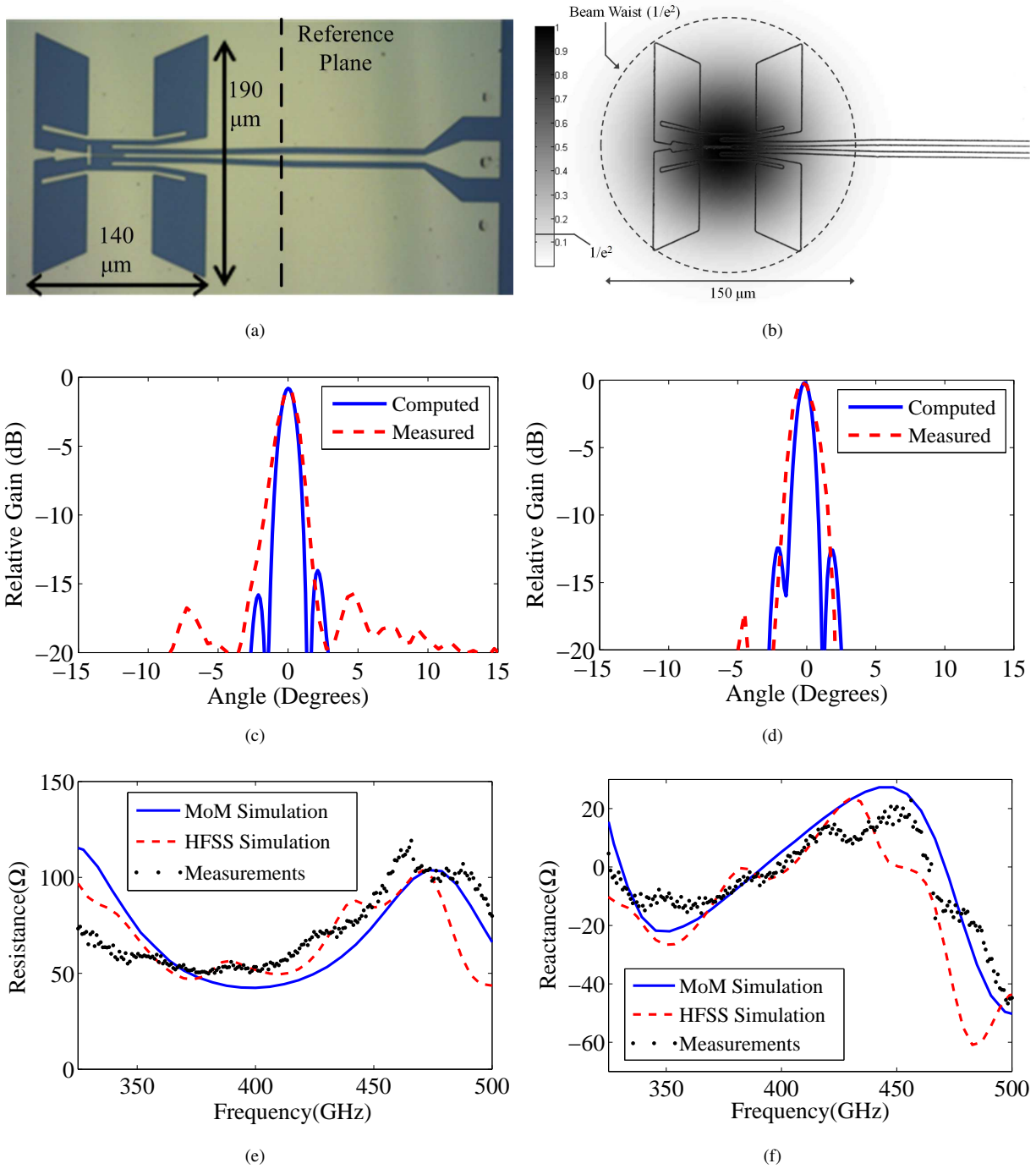We also note that as compared to contact probes, the non-

Fig. 4. Radiation pattern and impedance characterization of non-contact probe antenna using contact probes: (a) Micrograph of the on-chip non-contact probe antenna. (b) Illustration of the beam spot and the non-contact probe antenna.(c) Computed and measured *E*-plane pattern. (d) Computed and measured *H*-plane pattern. (e) Comparison of measured and computed antenna input resistance and (f) reactance.

contact probes are much less prone to misalignment. This is due to the "distributed" nature of coupling between the incident THz beam and the probe antenna. As seen in Fig. 4(b), signal coupling takes place over the large physical area of the incident beam and slight misalignment of the probe antenna under the beam spot (up to several micrometers at times) does not impact the magnitude or phase of the signal observed

on the CPW transmission line. This is in stark contrast to contact probe performance where contact point misalignment directly impacts the phase center of the signal on the CPW transmission line.

Furthermore, the quasi-optical nature of the setup makes it much less sensitive to vibrations, to a degree that no special vibration isolated probe station is required for our setup, which

is a major advantage over contact probe setups for sub-mmW characterization.

A. Broadband On-chip Slot Antennas for Non-Contact Testing

As mentioned earlier, a key feature of non-contact probes is the butterfly-shaped, broadband double-slot antennas that are integrated with the device under test on the same chip. We design and optimize the impedance and radiation pattern of the on-chip antennas, as in [15] to satisfy three key requirements: i) Widest bandwidth covering the operation band of the VNA frequency extender modules, ii) optimal impedance match to the on-chip CPW device environment and iii) optimal polarization and pattern match for robust quasi-optical coupling to the VNA ports. To do so, full-wave moment method (MoM) tools (developed in-house [16]) are used.

The characterization of non-contact probe antennas using conventional contact probes is shown in Fig. 4. Measured pattern of the butterfly antenna is also given in Fig. 4(b) in addition to the illustration of the beam-spot size on the focal plane of the hemispherical lens. As seen in Fig. 4(e) and 4(f), the input impedance is stable and varies less than $10\,\Omega$ around $50\,\Omega$ across the 325-500 GHz band.

In addition to the butterfly antennas connected to the input and output ports of the test device, several calibration standards are also needed to account for and factor out the repeatable errors in the measurement setup. To do so, we adopt a calibration technique used for high-frequency contact probes [12], as described in the Section III.

We remark that the butterfly-shaped broadband double-slot antenna design allows more than 2:1 bandwidth coverage which could enable measurements of the same DUT in multiple waveguide bands (e.g., 325-750 GHz) using the same test structure.

B. Multi-port Measurements and DC Biasing of Test Devices

Contact probe measurements in the sub-mmW band often require customized probe stations. Commercial probe stations are currently only available for two-port characterization due to physical size limitations of frequency extenders and the associated micro-positioner mounts. Alternatively, the non-contact probe system presented here is readily expandable to multi-port measurements, owing to the compact quasi-optical system. Nevertheless, accurate on-wafer multi-port calibration is rather cumbersome and will be considered in a future publication.

The use of DC probes is still required for non-contact testing of active devices. Commercial contact probes offer an integrated bias-T option for testing active devices. Alternatively, DC contact probes are used alongside high-frequency contact probes to supply the generator voltage to the integrated circuits and transistor networks. Obviously, a DC bias-T is not an option for non-contact testing. However, as seen in Fig. 2, the non-contact test beams couple to the device environment from the back side of the device wafer. As such, the top side of the test wafer is available for supplying the DC power to the active components. It is thus rather straightforward to implement any DC biasing schemes with the non-contact probe setup. The
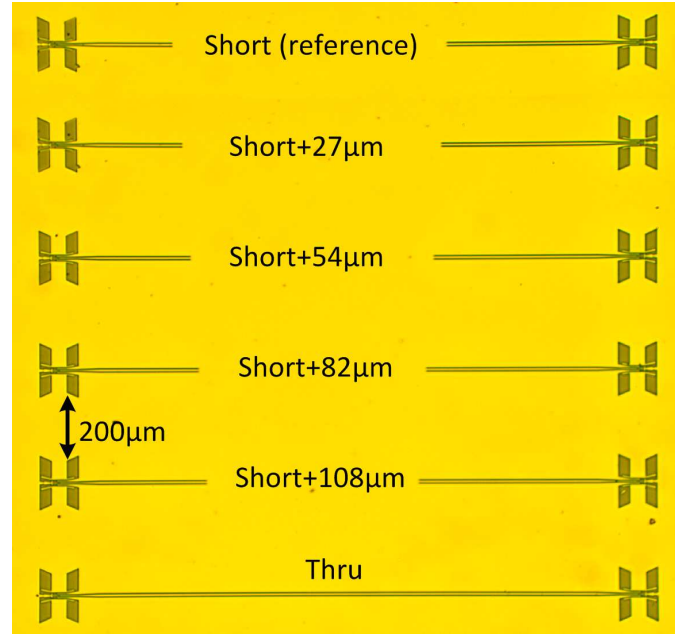

Fig. 5. Calibration standards for two-port calibration of the non-contact probe fabricated on a $500\,\mu$m GaAs substrate (physical separation between the probes is $200\,\mu$m as indicated).

only requirement is to place the DC probes onto the same platform as the test wafer, such that the DC probes and the test wafer move together under the high-frequency beam.

III. CALIBRATION OF NON-CONTACT THZ PROBE SETUP

Non-repeatable errors (such as the alignment of the on-chip antennas with the focal plane beam positions) are expected to have significant effect on the calibration accuracy. Since the beam spot on the planar antennas is rather sensitive to alignment errors (this is akin to the contact-probe landing accuracy), illumination of each non-contact probe during measurement is slightly different from one another. Preliminary studies show that displacements of the order of $10\,\mu$m in position result in a signal degradation approximately of 0.4 dB whereas $30\,\mu$m displacement adds 2 dB of uncertainty. In order to improve calibration accuracy under such measurement uncertainty, an over-determined calibration with more than three standards must be performed. Doing so, a sufficiently accurate calibration can be readily implemented using multiple, shorted CPW lines as the standards, as described previously in [12]. However, different from [12], the contact-probe landing pads are replaced by planar butterfly antennas in our setup. For example, non-contact probe antennas attached to 1-port calibration standards for 325-500 GHz band are shown in Fig. 5, where the lengths of short-ended transmission lines are chosen such that they add up to a full span around the Smith chart. For the 500-750 GHz band, the dimensions are simply scaled, that is, the shorted CPW line increment is shortened to $18\,\mu$m, which correspond same electrical length of $27\,\mu$m in the 325-500 GHz band.

The physical separation between the calibration standards can be chosen smaller than the wavelength at the lowest test frequency since the butterfly slot antennas have minimal in-
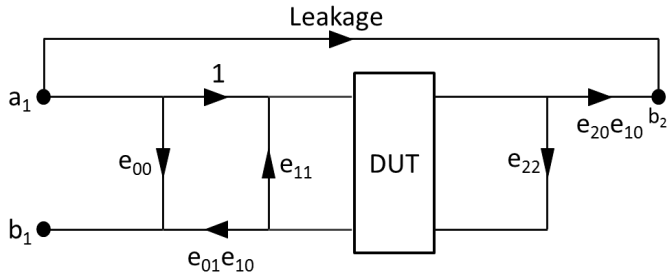
Fig. 6. Forward error model for transmitting/receiving port-1 and only receiving port-2, reproduced from [17]. The error terms in this model are extracted using the Q-SSS calibration procedure.

plane mutual coupling. Nevertheless, it is important to note that the on-chip antennas do take up some of the wafer real estate. However, the size of the non-contact probe antennas is similar to the landing pads of the contact probe measurements and modifying the quasi-optical alignment, the positions and the separation between the non-contact probe antennas can be changed arbitrarily. Thus, the additional on-chip real-estate needed for non-contact probe antennas can be kept to a minimum. We note however that a key requirement for the non-contact probe antennas is that they must be fabricated directly on the substrate since any additional fabrication layers would interfere with the incident beam impinging the antenna from the substrate side.

For two-port calibration of the non-contact probe setup, we adopted the Quick-Offset Shorts (Q-SSS) calibration method. This approach is akin to QSOLT (Quick-Short-Open-Load-Thru) method discussed in [18]. We note however that this is the first-time implementation of Q-SSS method for two-port device characterization.

As noted above, the separation between the input and output non-contact probe antennas can be designed to accommodate a wide range of test devices. However, due to the secondary reflections from the lens surface back to the focal plane, there is a small but observable leakage between on-chip probe antennas. To account for this leakage term, the error model in Fig. 6 is considered and the following two-port calibration process is implemented using a two-tier calibration:

1) First, the VNA frequency extenders are calibrated to the output waveguide flanges. For S_{11}, waveguide offset short calibration kit with three shorts (shims) is used. For S_{21}, a zero length thru measurement is performed. This calibration performed primarily to observe the correct time-domain signal during second tier calibration measurements. In addition, VNA time gating may be applied to further improve measurement accuracy by eliminating stray signals.

2) Next, we perform the on-chip one-port calibration to determine error parameters (e_{00}, e_{11}, $e_{10} e_{01}$) using offset-short standards as described in [12],

3) Subsequently, the leakage term is determined by measuring the S_{21} of the longest offset short standard. Since this is typically measured by terminating reference plane of the first port with matched load. As such, there is a weak overestimation on the leakage term since some

part of the energy reflected back from the shorted CPW section is coupled to the second port. We also note that characterization and mitigation of probe crosstalk can be quite complex, particularly with bulky probe tips at sub-mmW frequencies. In our non-contact probe setup, the crosstalk between the input and output ports is minimal (but of course not negligible) since the coupling between the in-plane slot antennas is very small. In our initial experiments, we indeed noticed that for small devices where the input and output calibration planes are very close to each other (e.g., less than one tenth of a wavelength in overall length), multi-mode crosstalk typically dominates the measured data. To alleviate such issues, well-separated calibration planes should be used.

4) Finally, the error parameters e_{22} and $e_{20} e_{10}$ are determined using the flush through measurement and the previously extracted 1-port and leakage error terms.

In addition, time-gating was employed to remove the etalon effect in the physical path of the probe beam due to the features of the setup that lead to high reflections in raw measurements. Typically, the initial reflection from the diagonal horn antenna and the secondary reflection from the on-wafer slot antenna can amplify non-repeatable errors in the quasi-optical system, making the measured raw data more susceptible to the non-repeatable errors, thus yielding high calibration residuals. We note, however, that these unwanted reflections are well-separated in time, allowing us to use a wide time-gate to minimize their impact on the overall calibration and measurements. For the data shown throughout the paper, a rather large (i.e., 200 picosecond) Kaiser-type time window was chosen to filter out such artifacts in the final measured data.

In the current realization of the non-contact probe setup, the quasi-optical alignment is fixed, resulting in fixed probe antenna positions on the wafer. As such, the standard TRL calibration is not readily applicable. As an alternative, the self-defined Line-Reflect-Reflect-Reflect (LRRR) calibration [19] is more commensurate with this implementation. Nevertheless, characterization of different test devices with varying sizes can easily be carried out using multiple calibration standards that ensure the relative position of the calibration planes for each device.

During the calibration measurements, each standard is measured only once and a least-squares algorithm [20] is used to extract one-port error terms from five measurements of standards. In order to check the self-consistency of calibration standards, each standard is re-measured, keeping the remaining standards measurements as the calibration set. Figure 7(a) shows the comparison of "re-measured" standards with full-wave (HFSS) simulations on the Smith chart for the 325-500 GHz band. A similar procedure for the 500-750 GHz results in the response shown in Fig. 7(b) illustrating the accuracy and repeatability of the non-contact calibration: The re-measured response of the calibration standards was within 0.1 dB in magnitude and 3 degrees in phase for the 325-500 GHz band and 0.2 dB and 5 degrees for the 500-750 GHz band, respectively.

In order to estimate one-port calibration residuals, we
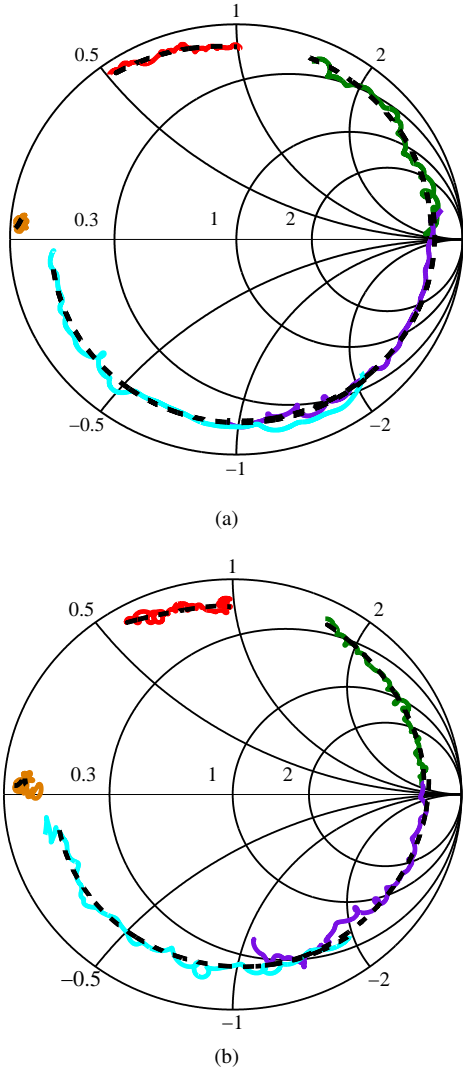
(a)

(b)

Fig. 7. Smith chart representation of re-measured standards: Dashed lines are HFSS simulations, thin solid lines are measurements: (a) 325-500 GHz (b) 500-750 GHz

Fig. 8. Measured S-parameters for contact and non-contact probes between the VNA extender waveguide and reference plane. The S_{21} data corresponds to the insertion loss of the respective probe setup.

followed the procedure presented in [20] and measured the error terms of the non-contact probe 25 times over a time period of two hours in the 500-750 GHz band. The standard deviation in the error terms were used as the diagonal elements of covariance matrix of the error network. Following the algebraic procedure outlined in [20], we estimate the residual directivity (δ) to be around -40 dB, whereas the residual source match (μ) is approximately -15 dB. Also, the residual reflection tracking (τ) is around -30 dB, which illustrates the efficacy of the calibration. The performance of the non-contact probes is expected to further improve for lower-frequencies since the non-repeatable errors are typically much reduced.

IV. INSERTION LOSS CHARACTERIZATION

Since the dynamic range of the VNA frequency extenders deteriorate at high frequencies, the insertion loss of conventional high-frequency probes is an important performance parameter for accurate device characterization in the mmW and THz bands. For commercial contact probes, the insertion
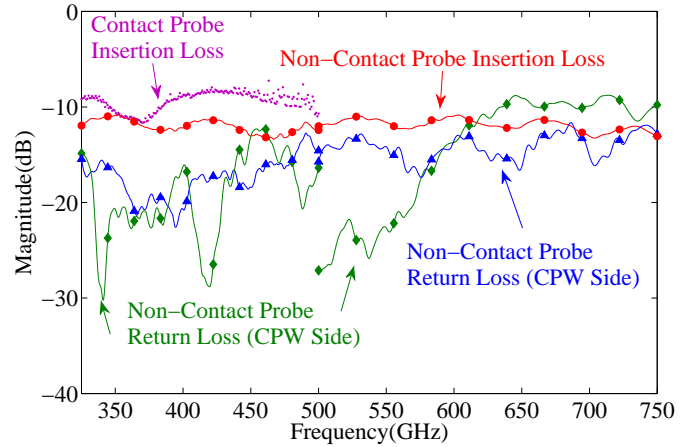
loss ratings range from 7-10 dB in the 0.3-1 THz band. Probe insertion loss can be measured using the two-tier calibration procedure discussed above. In the first-tier calibration, the reference plane is the waveguide port of the frequency extender unit. In the second-tier, one-port calibration with five delayed shorts is performed. The resulting error parameters obtained in the second-tier calibration corresponds to the S-parameters of the non-contact probe, as shown in Fig. 8. For the non-contact THz probes, we observe approximately 12 dB of insertion loss, increasing up to 13 dB at 750 GHz. Overall, the system losses include: i) 3 dB of Gaussicity mismatch, ii) 3 dB due to reflection and material losses from the high resistivity Si lens, and iii) 1 to 2 dB loss due to metallic losses in coplanar waveguides. Thus, the total calculated losses range from 7 to 8 dB over 325-750 GHz band.

The above estimates are for a perfectly aligned quasi-optical link. However, achieving a perfect alignment is not straightforward. As a result, approximately 4 dB of extra losses were experimentally observed which can be attributed to the alignment mismatches in the quasi-optical setup.

As seen in Fig. 8, the insertion loss of the non-contact probes is 4 dB higher that of the commercially available contact probes for the 325-500 GHz band. Thus, the overall reduction in the dynamic range due to the non-contact probes is 8 dB lower in comparison to contact probes. Considering the dynamic range of frequency extenders are typically better than 80 dB, the overall dynamic range of the non-contact probe setup is over 50 dB in the 325-750 GHz band.

Another advantage of non-contact probe setup is that it exhibits constant insertion loss with increasing frequency due to its quasi-optical nature. This is particularly advantageous when testing frequencies higher than 1 THz where there are no existing on-chip device testing solutions. Practically, the same quasi-optical setup can be used to characterize devices starting from mmW to THz frequencies (60 GHz to 3 THz) without any significant change in the system losses.

Furthermore, unlike the contact probes requiring sophisticated control on the testing process (such as applied contact force, over-travel distance, planarity, etc.), the non-contact
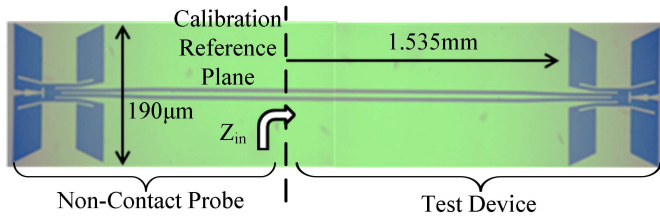
Fig. 9. Through connected non-contact probe pair. The test device is the antenna (325-500 GHz) with 1.535 mm CPW line on the right

probes are easily manipulated without any concern of damaging expensive test equipment. Thus, there is no issue of wear and tear on the non-contact probes. The only requirement is to fabricate the non-contact probe antennas together with the test device on the same wafer, much like the landing pads for contact probes.

One of the other advantages of the proposed non-contact probes is a significant reduction of the overall cost of the testing setup. For instance, the price of contact probes starts with approximately $3000 at WR 12.2 (60-90 GHz) and increases up to $19,000 at WR 1.5 (500-750 GHz) as of July 2014. Thus, a two-port contact probe assembly covering the 60 GHz to 1.1 THz band typically costs over $100,000, not including the cost of the high-end probe stations and vibration isolation optical tables that must be used. On the contrary, the cost of the non-contact probe setup described above is a small fraction of this number.

V. On-Wafer Device Characterization Using Non-Contact Probes

To demonstrate the accuracy and effectiveness of the proposed non-contact test setup, we first consider the impedance of the butterfly shaped double-slot antenna at 325-500 GHz and at 500-750 GHz, respectively. For this purpose, a through connected non-contact probe pair is used, as shown in Fig. 9. Here, one of the probe antennas is considered as a test device whereas the second antenna forms the non-contact probe tip. The characterization is performed after one-port calibration using the standards shown in Fig. 5. The real and imaginary parts of the measured antenna impedance are compared with the full-wave simulation data in Fig. 10(a) and Fig. 10(b), respectively. We note that the difference between the computed and measured impedance values are primarily due to variances in the microfabrication processes. Small variations in the micro-fabrication can result in significant impact in sub-mmW device performance. For example, the e-beam evaporator system we used exhibited a 15% tolerance for gold deposition. To assess the impact of such variations on performance, we conducted a set of full-wave simulations of the antenna shown in Fig. 9 using different metallization thicknesses. In summary, a ± 50 nm variation in metallization thickness was observed to cause up to ± 10 Ohms variation in antenna impedance. As such, the variations between the measured and simulated results shown in Fig. 10 and 11 are well within the repeatability limits of the micro-fabrication process for such high-frequency measurements. Furthermore, as seen in Fig. 10(a) and 10(b), the accuracy of non-contact probe

measurements and conventional contact probe measurements are comparable. For these measurements, the number of VNA data points was 3201 and the IF bandwidth was set to 700 Hz.

The real and imaginary parts of the measured and the simulated antenna impedance for the 500-750 GHz band for three independent measurements are shown in Fig. 11(a) and Fig. 11(b), respectively. Again, excellent agreement is obtained, demonstrating the accuracy and repeatability of the non-contact probes setup.

To demonstrate two-port non-contact measurements, we implemented two representative passive components on GaAs, namely a mismatched thru (Beatty standard) and a bandpass filter, as depicted in the insets of Fig. 12. For the Beatty standard characterization, ten independent measurements were collected and the agreement between the measured results and the simulations are with 0.5 dB for S_{21}. However, the measured S_{11} is more sensitive to variations due to low signal levels. Nevertheless, as seen in Fig. 12(a), the S_{11} characterization performance of the non-contact probes is similar to that of the contact probes at this frequency band.

In Fig. 12(b), the measured response of a capacitively end-coupled bandpass filter is shown. As seen, the difference between simulated and measured response is higher than the previous case since the filter performance is much more sensitive to the fabrication uncertainties. In addition, a slight shift in the center frequency was observed due to such fabrication uncertainties.

The ripples in the measured S_{21} in Fig. 12(b) are due to the calibration residuals rather than the time-gating artifacts. These residuals are particularly high for transmission measurements since only a single calibration standard is used to extract the corresponding error terms. The effect of the residuals is not noticeable for larger signals, as shown in Fig. 12(a).

A more rigorous treatment of measurement repeatability using non-contact probes is currently under way and will be subject of a future paper.

In light of the above performance validations, a short list of advantages of the non-contact probe can be summarized as follows:

- Scalability: The non-contact probe concept can be extended well into the THz band, the losses and wear/tear issues do not increase with frequency
- Longevity: There is no inherent limitation to te number of measurements since there is no degradation of the probe equipment or the test wafer.
- Modularity: The quasi-optical sub-system and the VNA is used for the entire frequency band. The frequency extender modules are replaced for each sub-band.

VI. Conclusion

We presented the first time validation of a new non-contact measurement setup for on-chip characterization of THz-frequency devices and integrated circuits. The proposed approach is simple, effective and easily scalable in THz range and beyond. Owing to the non-contact nature, the new probe is free from fragility and wear/tear issues of traditional contact-based probes. Same quasi-optical testbed can be used from
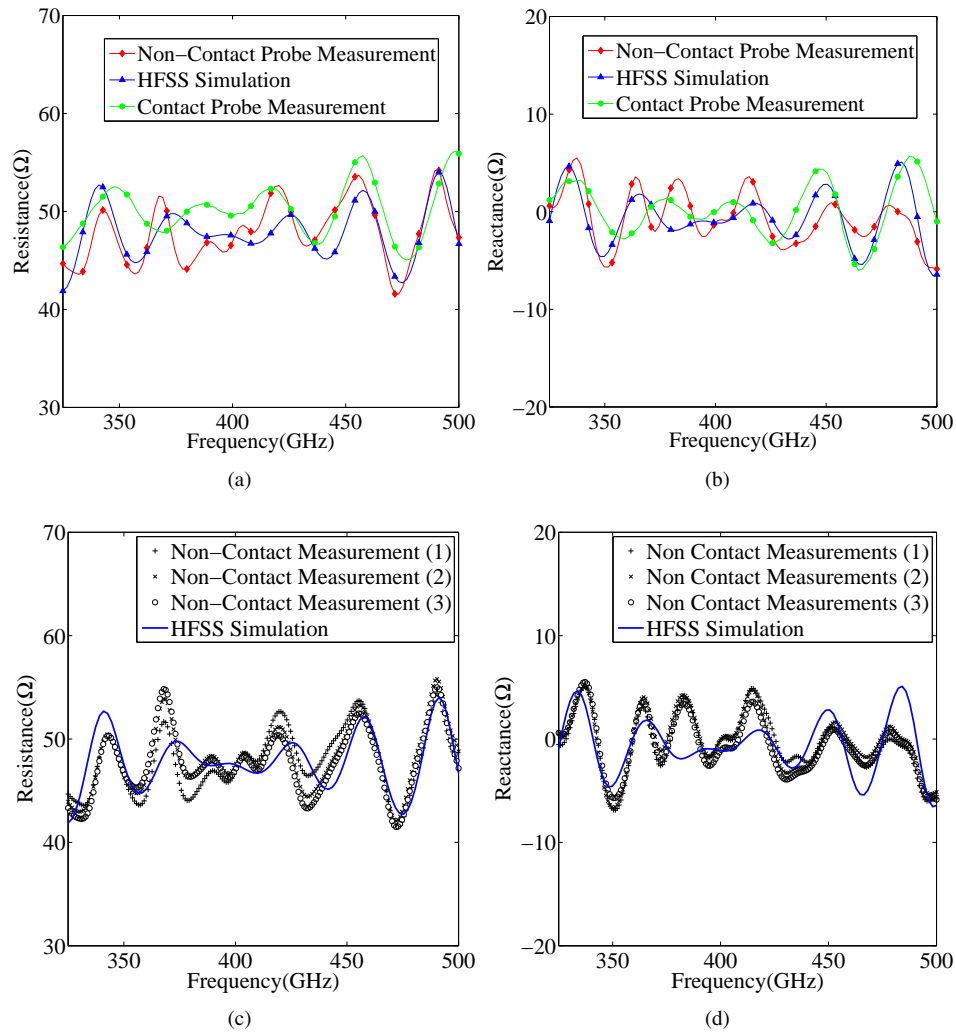
Fig. 10. Comparison of measured (non-contact and contact) and simulated impedance for the non-contact probe antenna in the 325-500 GHz band:(a) Resistance (b) Reactance (c) Scatter plot of three independent measurements of antenna resistance and HFSS simulation (d) Scatter plot of three independent measurements of antenna reactance and HFSS simulation
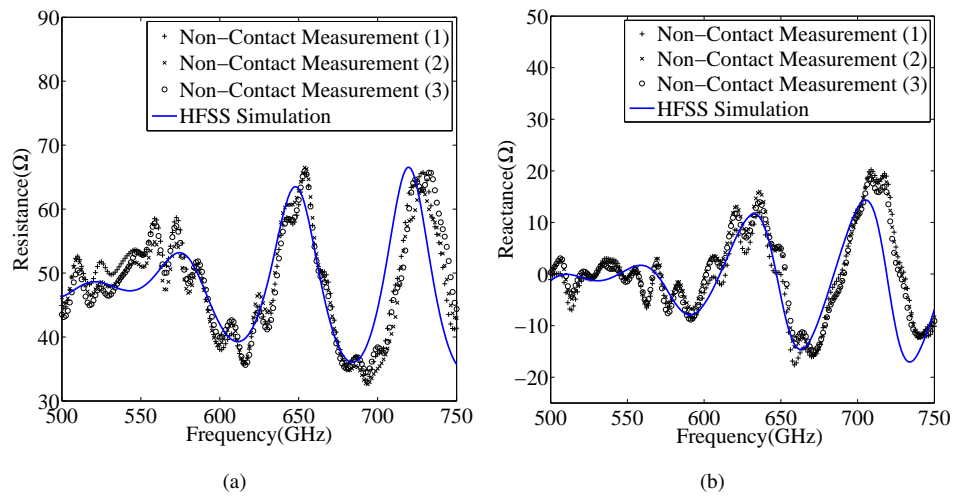

Fig. 11. Comparison of measured (scatter plot of three independent measurements) and simulated impedance for the non-contact probe antenna in the 500-750 GHz band:(a) Antenna resistance (b) Antenna reactance.
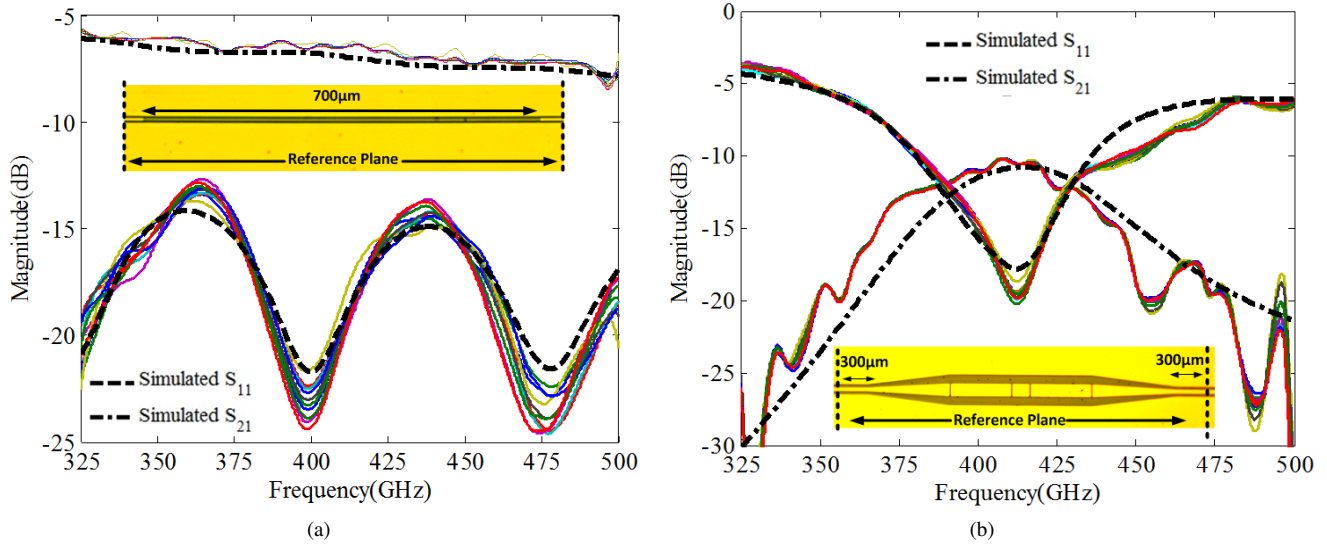
Fig. 12. On-chip passive components for two-port non-contact characterization: (a) A Beatty standard (mismatched through). The photograph is shown in the inset. (b) A capacitively end-coupled bandpass filter (photograph is shown in the inset). We note that the presence of $300\,\mu$m CPW line between the measurement reference plane and the input and output ports of the filter results in $3\,$dB extra loss.

mmW band to THz by simply scaling the probe antennas. An overall insertion loss as low as $12\,$dB has also been demonstrated. This new technique is particularly useful for testing devices beyond $1.1\,$THz where contact suffer from fragility and extreme costs.

ACKNOWLEDGEMENT

REFERENCES

[1] P. Siegel, "Terahertz technology," *IEEE Transactions on Microwave Theory and Techniques*, vol. 50, no. 3, pp. 910–928, March 2002.

[2] J.-H. Son, "Terahertz electromagnetic interactions with biological matter and their applications," *Journal of Applied Physics*, vol. 105, no. 10, p. 102033, May 2009.

[3] J. Federici, B. Schulkin, F. Huang, F. Gary, R. Barat, F. Oliveira, and D. Zimdars, "THz imaging and sensing for security applications-explosives, weapons and drugs," *Semicond. Sci. Technol.*, vol. 20, no. 7, p. S266, June 2005.

[4] H.-J. Song and T. Nagatsuma, "Present and future of terahertz communications," *IEEE Transactions on Terahertz Science and Technology*, vol. 1, no. 1, pp. 256–263, September 2011.

[5] V. Radisic, K. Leong, X. Mei, S. Sarkozy, W. Yoshida, and W. Deal, "Power amplification at 0.65 THz using InP HEMTs," *IEEE Transactions on Microwave Theory and Techniques*, vol. 60, no. 3, pp. 724–729, March 2012.

[6] M. Dyakonov and M. Shur, "Detection, mixing, and frequency multiplication of terahertz radiation by two-dimensional electronic fluid," *IEEE Transactions on Electron Devices*, vol. 43, no. 3, pp. 380–387, March 1996.

[7] K. Leong, W. Deal, V. Radisic, X. B. Mei, J. Uyeda, L. Samoska, A. Fung, T. Gaier, and R. Lai, "A 340-380 GHz integrated CB-CPW-to-Waveguide transition for sub millimeter-wave MMIC packaging," *IEEE Microwave and Wireless Components Letters*, vol. 19, no. 6, pp. 413–415, June 2009.

[8] T. Reck, L. Chen, C. Zhang, A. Arsenovic, C. Groppi, A. Lichtenberger, R. Weikle, and N. Barker, "Micromachined probes for submillimeter-wave on-wafer measurements part I: Mechanical design and characterization," *IEEE Transactions on Terahertz Science and Technology*, vol. 1, no. 2, pp. 349–356, November 2011.

[9] Q. Yu, M. Bauwens, C. Zhang, A. Lichtenberger, R. Weikle, and N. Barker, "Improved micromachined terahertz on-wafer probe using integrated strain sensor," *IEEE Transactions on Microwave Theory and Techniques*, vol. 61, no. 12, pp. 4613–4620, December 2013.

[10] C. Caglayan, G. C. Trichopoulos, and K. Sertel, "On-wafer device characterization with non-contact probes in the THz band," *IEEE Antennas and Propagation Society International Symposium (APSURSI)*, pp. 1134–1135, July 2013.

[11] ——, "Non-contact probes for device and integrated circuit characterization in the THz and mmW bands," *IEEE International Microwave Symposium*, pp. 1–3, June 2014.

[12] L. Chen, C. Zhang, T. Reck, A. Arsenovic, M. Bauwens, C. Groppi, A. Lichtenberger, R. Weikle, and N. Barker, "Terahertz micromachined on-wafer probes: Repeatability and reliability," *IEEE Transactions on Microwave Theory and Techniques*, vol. 60, no. 9, pp. 2894–2902, July 2012.

[13] A. Love, "The diagonal horn antenna," *Microwave Journal*, vol. 5, pp. 117–122, March 1962.

[14] D. Filipovic, S. Gearhart, and G. Rebeiz, "Double-slot antennas on extended hemispherical and elliptical silicon dielectric lenses," *IEEE Transactions on Microwave Theory and Techniques*, vol. 41, no. 10, pp. 1738–1749, October 1993.

[15] G. C. Trichopoulos, H. Mosbacker, D. Burdette, and K. Sertel, "A broadband focal plane array camera for real-time THz imaging applications," *IEEE Transactions on Antennas and Propagation*, vol. 61, no. 4, pp. 1733–1740, April 2013.

[16] K. Sertel and J. L. Volakis, *Integral Equation Methods for Electromagnetics*. Scitech Publishing Inc., April 2012.

[17] R. B. Marks, "Formulations of the basic vector network analyzer error model including switch-terms," *50th ARFTG Conference Digest-Fall*, vol. 32, pp. 115–126, December 1997.

[18] J. P. Dunsmore, *Handbook of Microwave Component Measurements with Advanced VNA Techniques*. Wiley, October 2012.

[19] I. Rolfes and B. Schiek, "Self-calibration procedures for vector network analyzers on the basis of reflection standards," *33rd European Microwave Conference*, vol. 1, pp. 93–96, October 2003.

[20] K. Wong, "Uncertainty analysis of the weighted least squares VNA calibration," *64th ARFTG Microwave Measurements Conference*, pp. 23–31, December 2004.